Supporting Information for "Mechanisms of Fast Walker Circulation Responses to CO_2 Forcing"

Kezhou Lu[1], Jie He[1], Boniface Fosu[1], and Maria Rugenstein[2]

[1]School of Earth and Atmospheric Sciences, Georgia Institute of Technology, GA, USA

[2]Department of Atmospheric Science, Colorado State University, CO, USA

Contents of this file

Figures S1 to S22

Introduction

Fig. S1 illustrates the design of CESM1 LE. Fig. S2 shows that the fast central Pacific cooling is independent of the number of the ensemble experiments. Fig. S3 the scaling analysis of the column integrated SST tendency equation. Fig. S4 and Fig. S5 show the relative and absolute changes and in surface wind and surface temperature for 27 CMIP5 models after quadrupling CO_2. Fig. S6 demonstrates the fast TS and surface wind changes in CESM1 LE. Fig. S7 shows the changes in 500 hPa pressure velocity in the first two years, year five to year 15, and year 91 to year 120 after quadrupling CO_2. Fig. S8 lists the initial ENSO state at the time of quadrupling for each CMIP5 model. Fig. S10 shows the relationship between ENSO intensity and initial wind anomalous easterlies over the Pacific warm pool. Fig. S10 demonstrates the relationship between land-sea warming contrast and anomalous easterlies in the warm pool region. Fig. S11 shows changes in convection and surface wind in AMIP simulations. Fig. S12 to Fig. S18 show the coupling between each individual terms when evaluating the strength of air-sea coupling. Fig. S19 and Fig. S20 show the slow response of TS, surface wind, and subsurface ocean temperature. Fig. S21 describes the timeline of the changes of tropical circulation. Fig. S22 shows the comparison between observational air-sea coupling and modeling results in CMIP5 historical simulations.

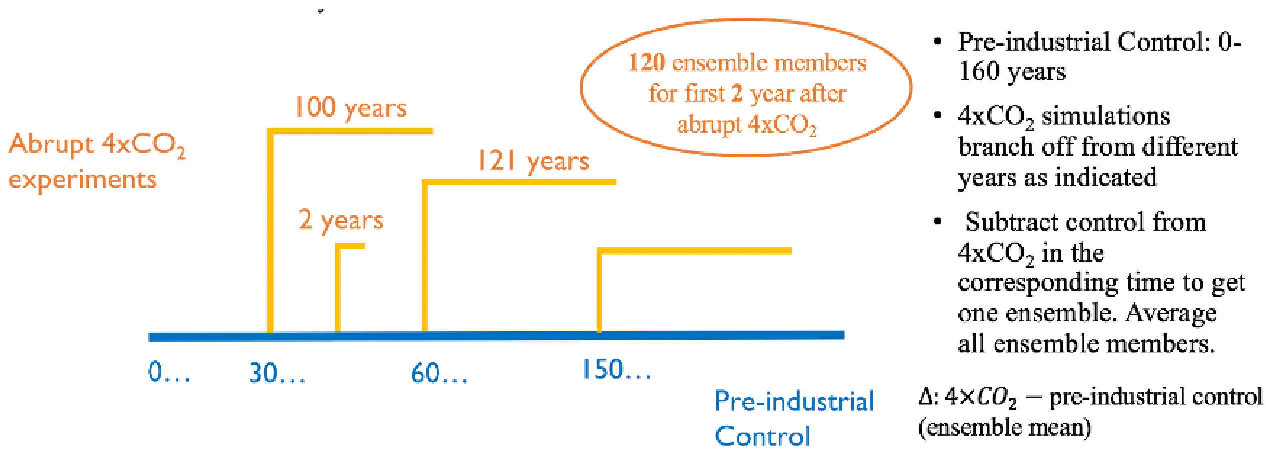

Figure S1. Sketch of the design of CESM1 LE. We branch off 120 abrupt $4\times CO_2$ experiments with different durations from the same parent pre-industrial control run. Then we subtract the control from the $4\times CO_2$ in the corresponding time step to produce one ensemble. This step is repeated 120 times to produce 120 ensemble differences and the mean changes are averaged across all ensemble differences.

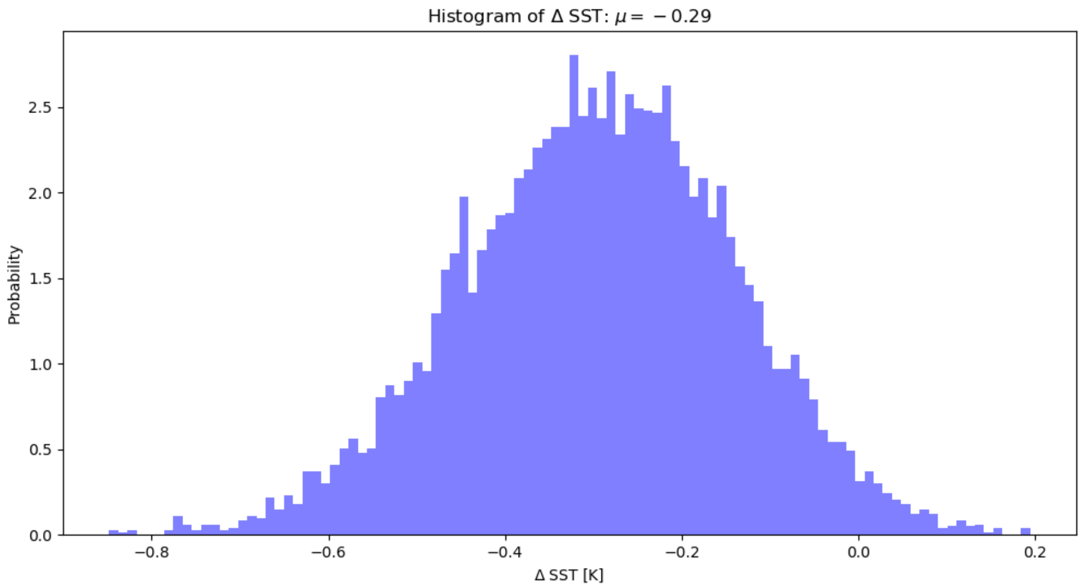

Figure S2. The central Pacific cooling in the fast response period is independent of the ensemble numbers of the abrupt $4 \times CO_2$ experiment. We randomly pick 14 unique ensembles from 120 CESM1 abrupt $4 \times CO_2$ experiments and calculate the first two years of ensemble mean changes in SST in the Niño 3.4 region. This process is then repeated 5000 times to produce the above probability density function. As demonstrated from the above plot, most ensemble mean changes with only 14 ensembles still produce a cooling in the central equatorial Pacific.

Scaling analysis of the column integrated SST tendency equation

We perform the scaling analysis across the entire equatorial Pacific basin ($5^oS - 5^oN$, $150^oE - 270^oE$) from models' pre-industrial simulations. We use standard deviation along the time dimension (σ) to represent the prime terms. We approximate mixed layer depth as $H = 75\ m$, the length of the equatorial Pacific basin as $X = 13334\ km$, and the width of the basin as $Y = 1106\ km$.

The zonal advection terms are approximated as:

$$|\overline{u}\frac{\partial T'}{\partial x}| = \overline{U}\ \frac{\sigma(T_{east} - T_{west})}{X}\ ,\ |u'\frac{\partial \overline{T}}{\partial x}| = \sigma U\ \frac{\overline{(T_{east} - T_{west})}}{X} \tag{1}$$

"East" and "west" denote the east and west half of the equatorial Pacific basin. Similarly, we can approximate the meridional terms as:

$$|\overline{v}\frac{\partial T'}{\partial y}| = \overline{V}\ \frac{\sigma(T_{north} - T_{south})}{Y}\ ,\ |v'\frac{\partial \overline{T}}{\partial y}| = \sigma(V)\ \frac{\overline{(T_{north} - T_{south})}}{Y} \tag{2}$$

Take CCSM4 model as an example, the scaling analysis of each term can be summarized by the following table (unit is converted to [K/day] and absolute values are shown)

$\boldsymbol{\lvert SW'/\rho c_p h\rvert}$	$\lvert LW'/\rho c_p h\rvert$	$\lvert SH'/\rho c_p h\rvert$	$\boldsymbol{\lvert LH'/\rho c_p h\rvert}$	$\lvert w'(\overline{T}_e - \overline{T})/h\rvert$
0.0023	0.0006	0.0001	**0.0027**	0.0007
$\boldsymbol{\lvert \overline{w}(T'_e - T')/h\rvert}$	$\lvert \overline{u}\,\partial T'/\partial x\rvert$	$\boldsymbol{\lvert u'\,\partial \overline{T}/\partial x\rvert}$	$\lvert \overline{v}\,\partial T'/\partial y\rvert$	$\lvert v'\,\partial \overline{T}/\partial y\rvert$
0.0054	0.0003	**0.0014**	0.00005	0.00002

Figure S3. Scaling analysis for each term in the column-integrated SST tendency equation

The bolded terms are about one or two magnitudes higher than the others.

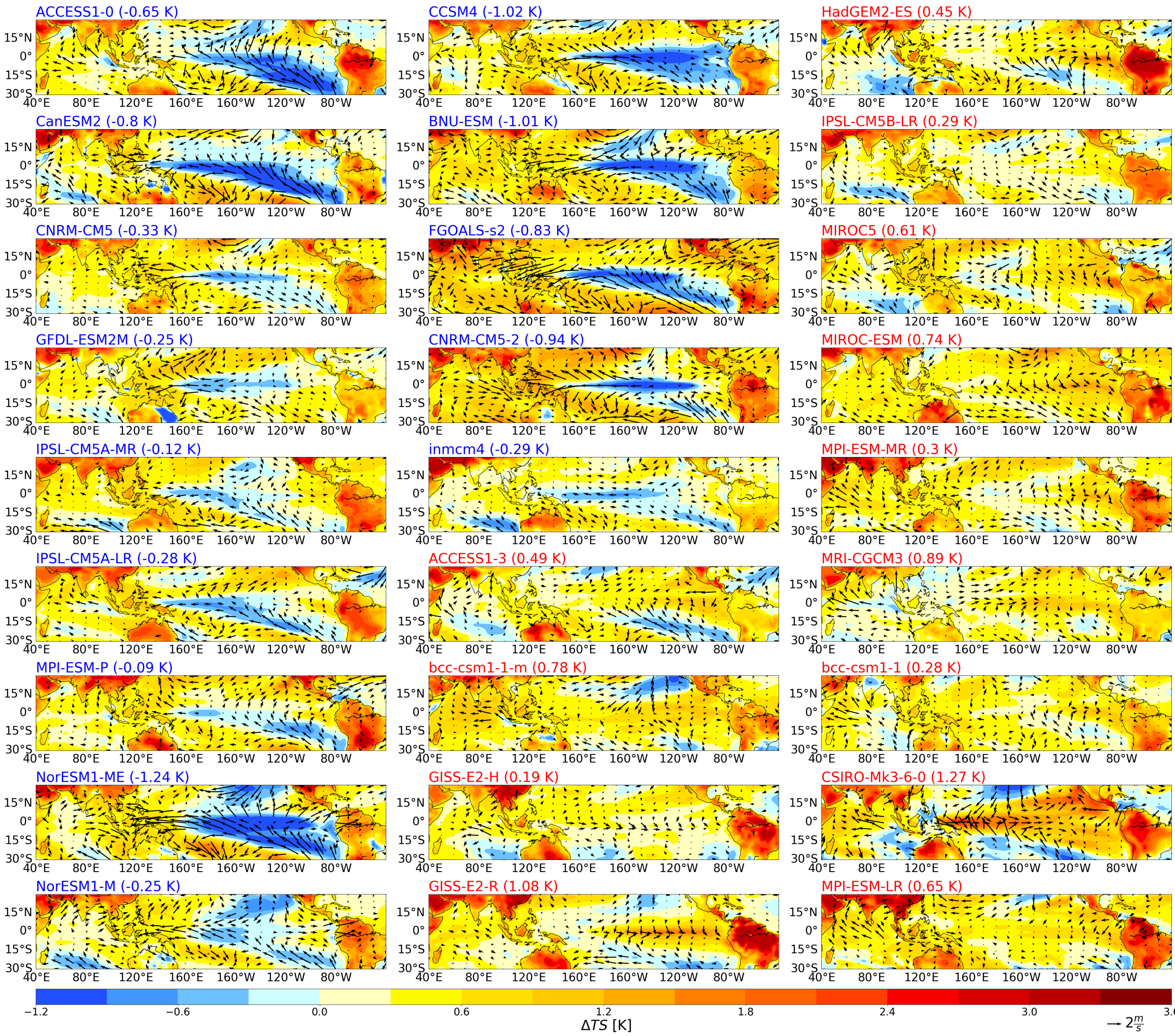

Figure S4. Fast relative response of TS (shadings) and surface wind (vectors) for 27 CMIP5 models. ΔTS is subtracted by the equatorial mean change of surface temperature. The name of individual model and its ΔSST in Niño 3.4 region are labeled on the top left of each plot. The CG models are labeled in blue and the WG models are in red.

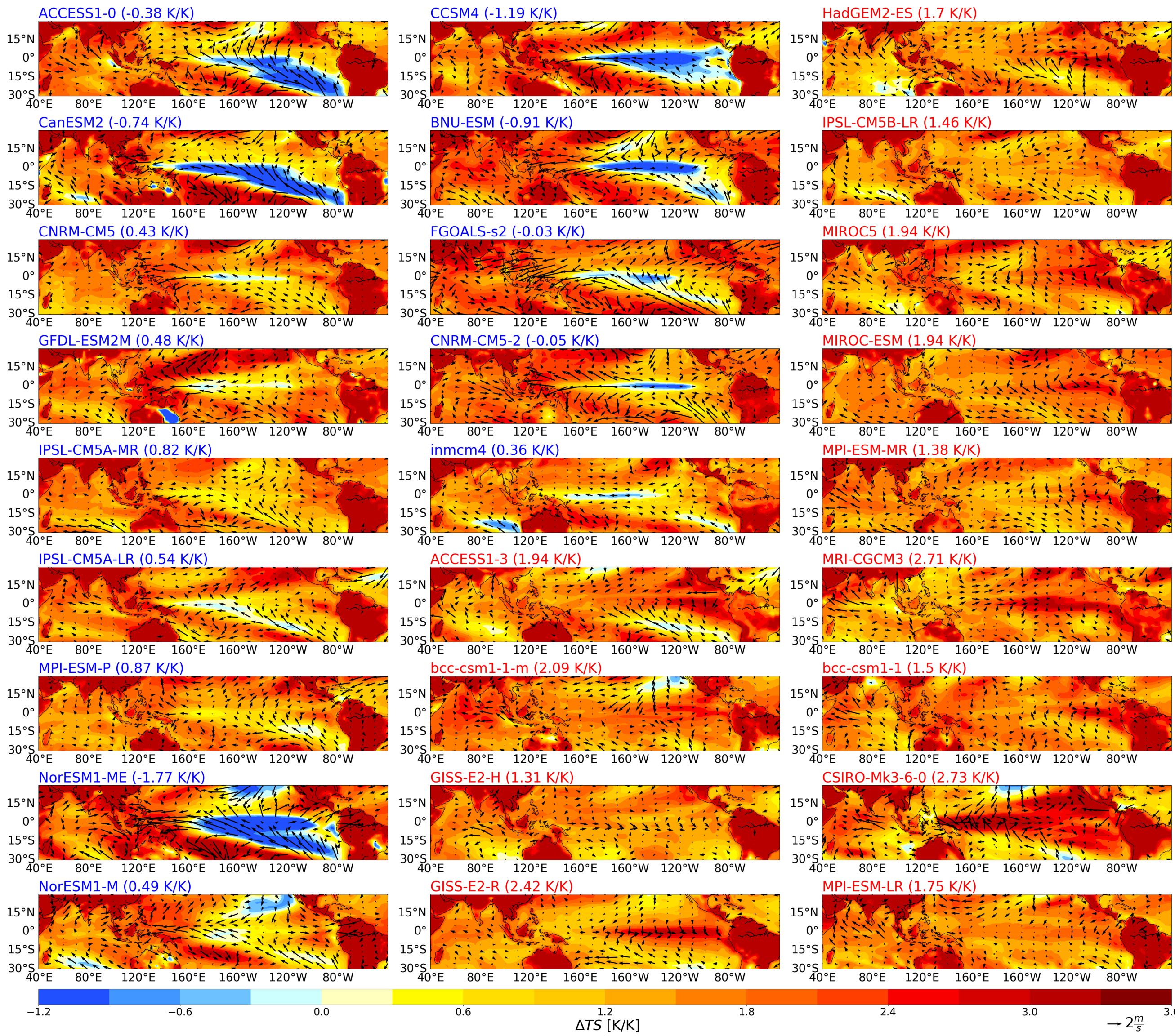

Figure S5. Same as Fig. S4 but for the absolute TS changes.

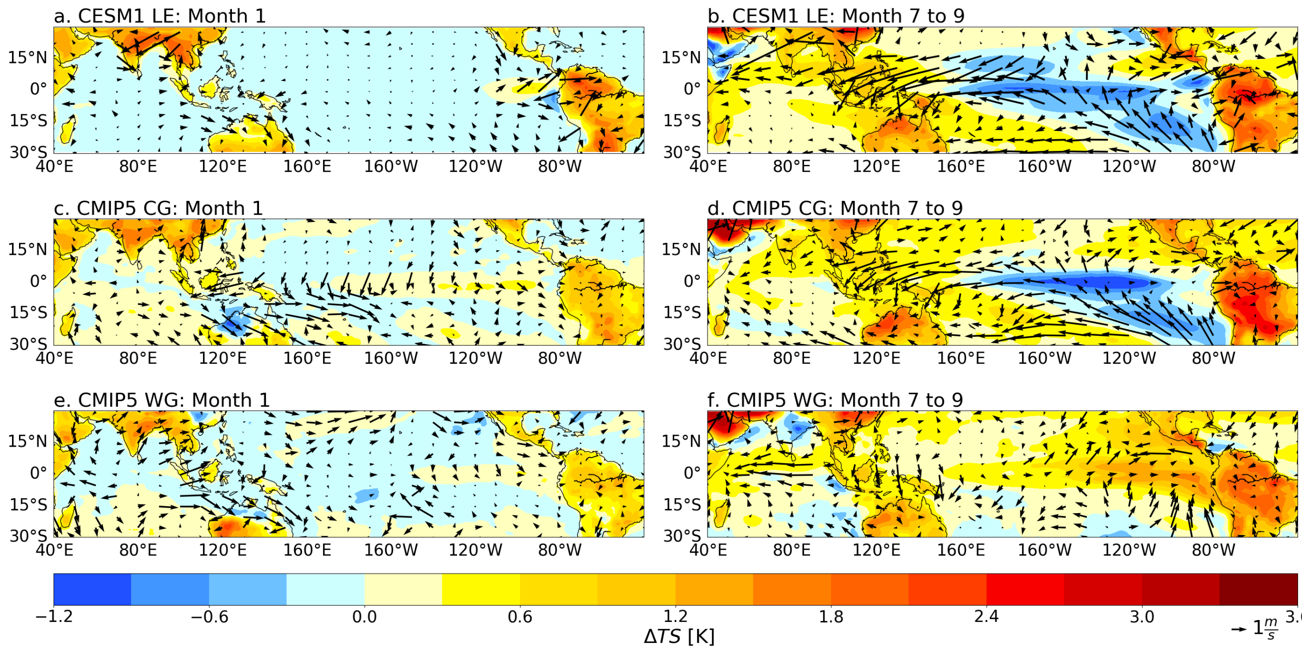

Figure S6. Relative changes in TS and surface wind in the first month (left column) and the seventh month (right column) after abrupt forcing for CESM1 LE (upper row), CMIP5 CG (middle row) and CMIP5 WG (bottom row).

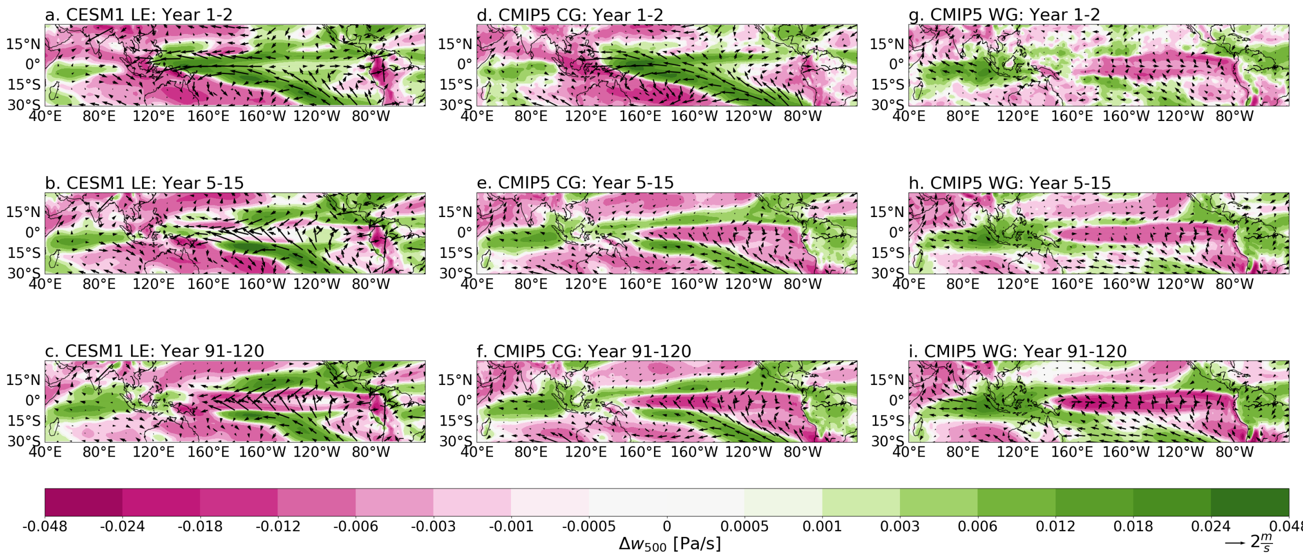

Figure S7. Changes in 500 hPa pressure velocity (shadings) and surface winds (vectors) at different time for CESM1 LE (a, b, c), CMIP5 CG (d, e, f) and CMIP5 WG (g, h, i).

Model	E or L	Intensity	Model	E or L	Intensity
CMIP5 CG					
NorESM1-ME	E	1.06	CCSM4		
BNU-ESM	L	-1.33	CanESM2		
ACCESS1-0			NorESM1-M		
CNRM-CM5-2			IPSL-CM5A-LR	E	1.34
FGOALS-s2			IPSL-CM5A-MR		
inmcm4	E	0.522	MPI-ESM-P	E	1.52
CMIP5 WG					
CNRM-CM5	E	1.00	GFDL-ESM2M		
GISS-E2-H			MPI-ESM-MR	E	1.22
IPSL-CM5B-LR			bcc-csm1-1		
HadGEM2-ES			MIROC5		
ACCESS1-3			IPSL-CM5A-LR		
MIROC-ESM			bcc-csm1-1-m	E	1.62
GISS-E2-R			MRI-CGCM3		
CSIRO-Mk3-6-0					

Figure S8. The initial ENSO state at the time of quadrupling for each CMIP5 model. An El Nino (La Niña) event is denoted as E (L). The E / L events are identified from the parent control simulations. The intensity of each event is calculated by averaging the Niño 3.4 SST over the E or L periods.

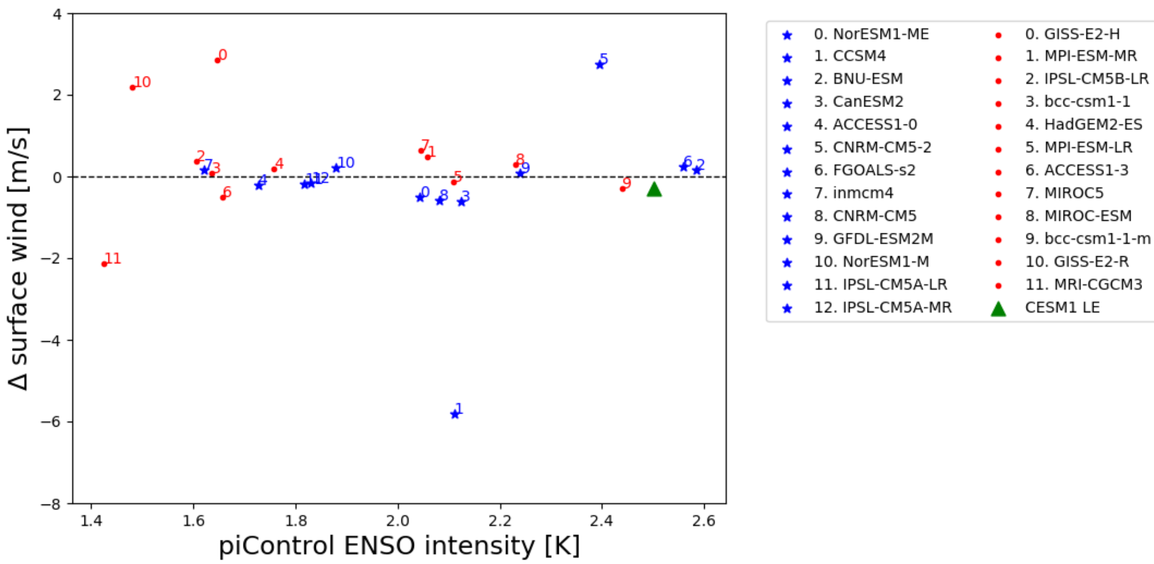

Figure S9. Changes in anomalous easterlies over the Pacific warm pool in the first month after abrupt CO_2 plotted against the ENSO intensity in the parent control run.

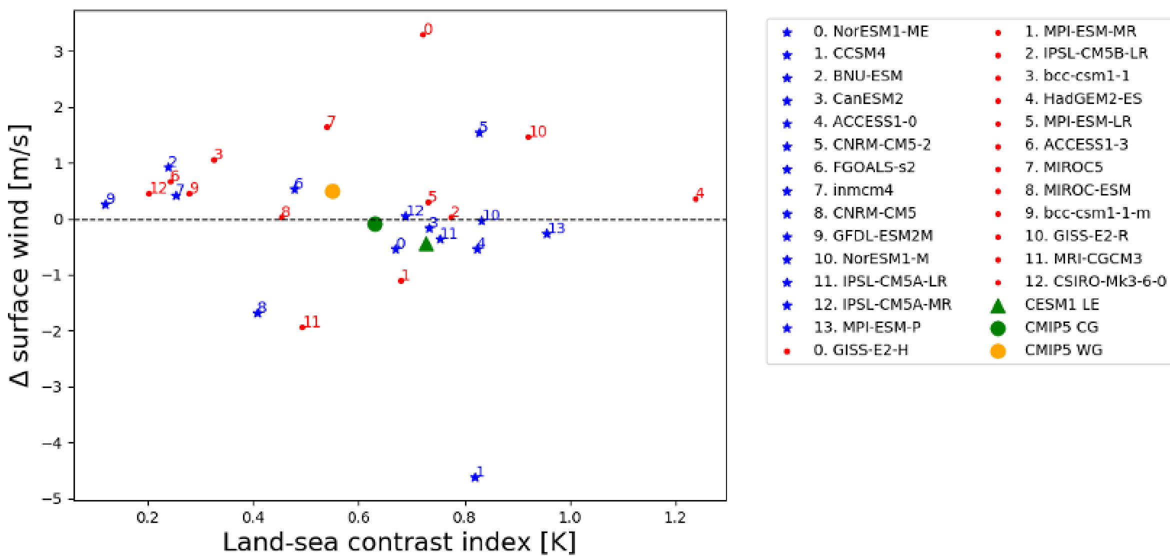

Figure S10. Changes in anomalous easterlies of the first 3 months after abrupt CO2 in the warm pool (region between $2^oS - 2^oN$ and $150 - 180^oE$) plotted against the land-sea warming contrast. The land-sea warming contrast index is defined as the temperature difference between all lands and ocean over $15^oS - 15^oN$. The Bjerknes feedback has not formed yet in the first three months.

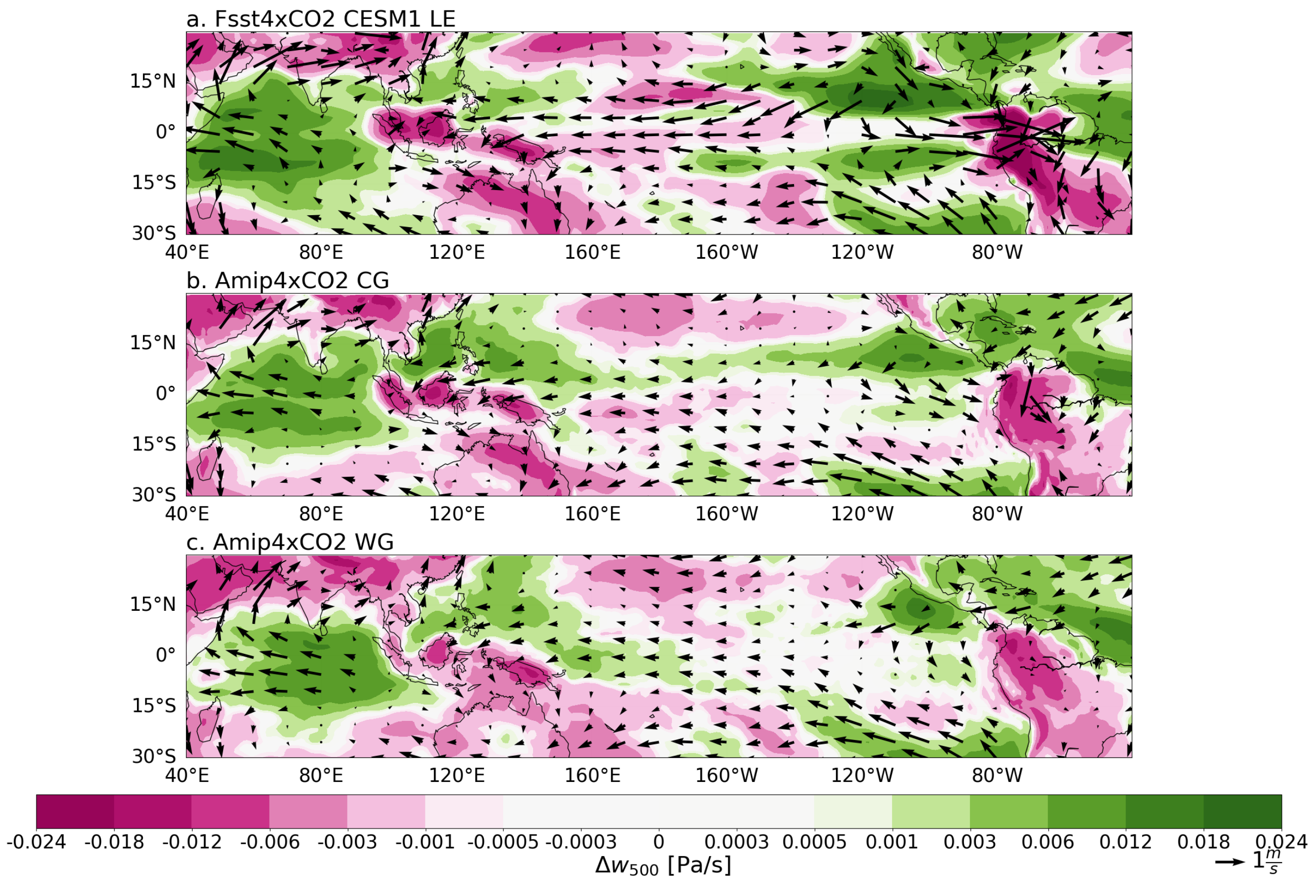

Figure S11. Changes in 500 hPa pressure velocity (shadings) and surface winds (vectors) for CESM1 LE (a), CMIP5 CG (b) and CMIP5 WG (c) in the Ami $4 \times CO_2$ simulations. The results are averaged over the entire 30 years. No air-sea coupling is included.

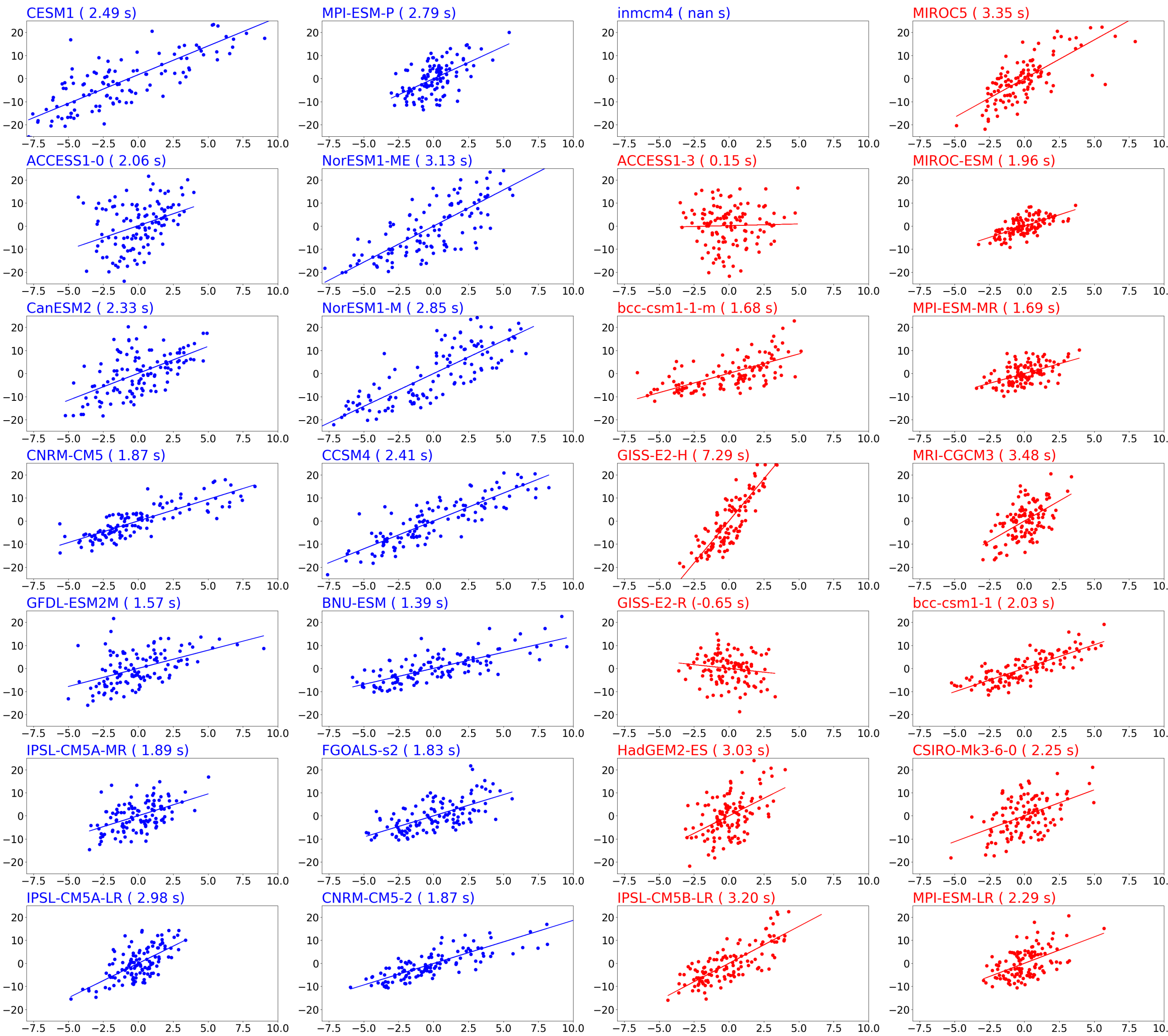

Figure S12. Relationship between 850-hPa zonal wind anomaly (m/s) in the western Pacific $(150 - 180^oE, 5^oS - 5^oN)$ and thermocline depth anomaly (m) in the eastern Pacific $(180 - 240^oE, 5^oS - 5^oN)$. The linear regression coefficient for each model is denoted inside of the parentheses.

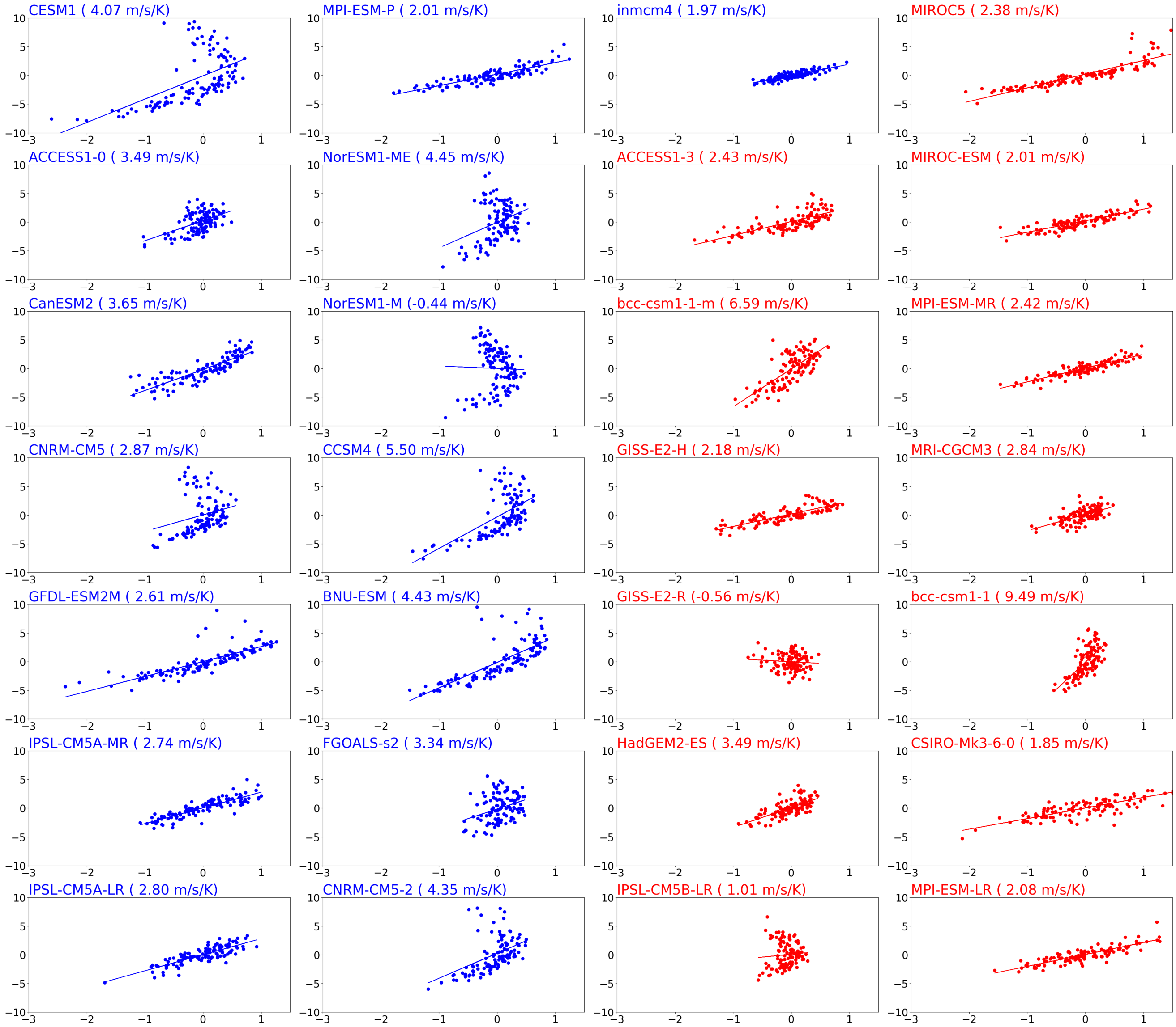

Figure S13. Same as Fig. S12, but for the relationship between SSTa (K) in and 850-hPa zonal wind anomaly (m/s) in the western Pacific ($150-180^oE, 5^oS-5^oN$).

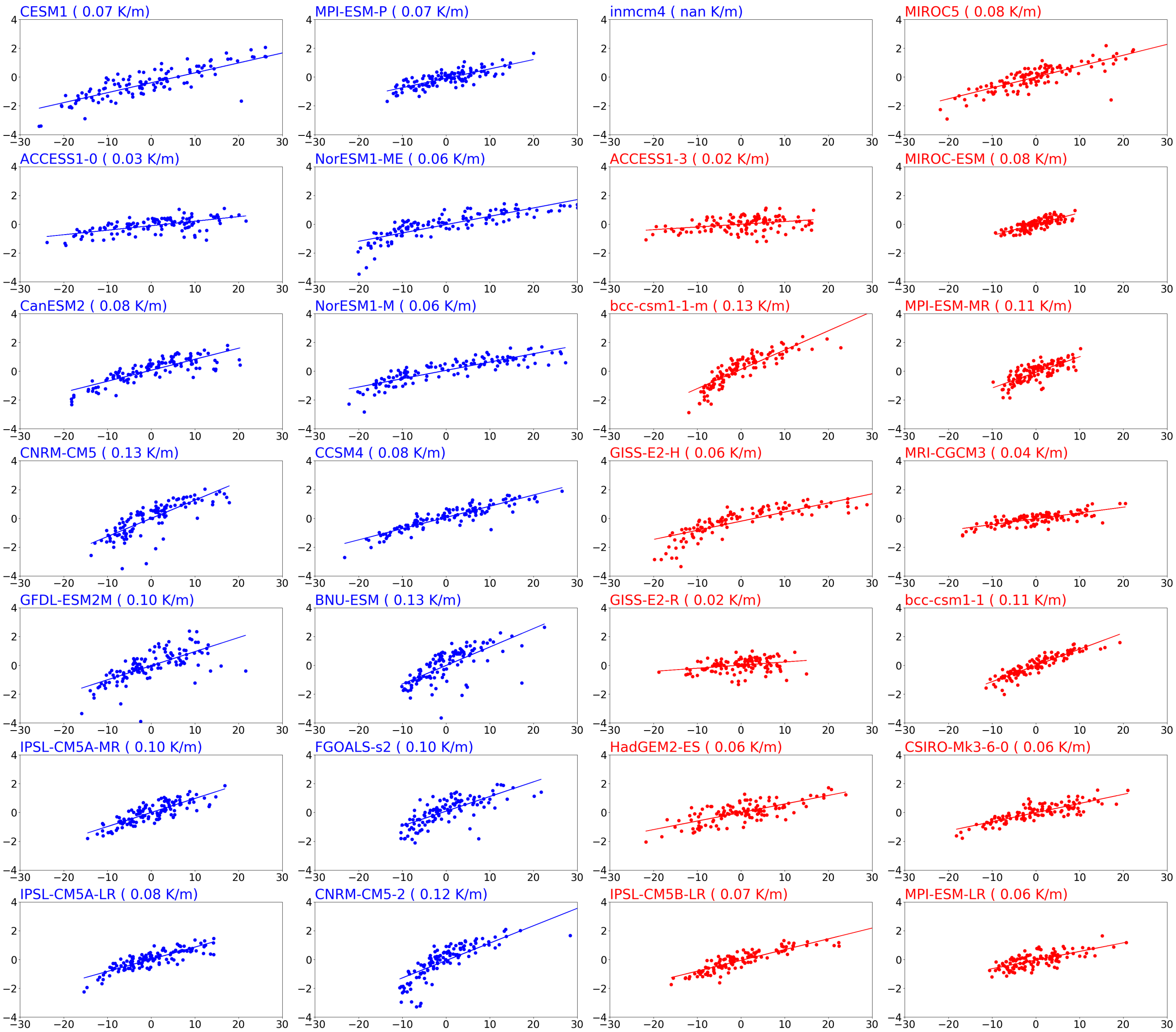

Figure S14. Same as Fig. S12, but for the relationship between thermocline depth anomaly (m) in the eastern Pacific ($180-240^oE, 5^oS-5^oN$) and subsurface temperature anomaly (K) at 75m in the western Pacific ($180-240^oE, 5^oS-5^oN$).

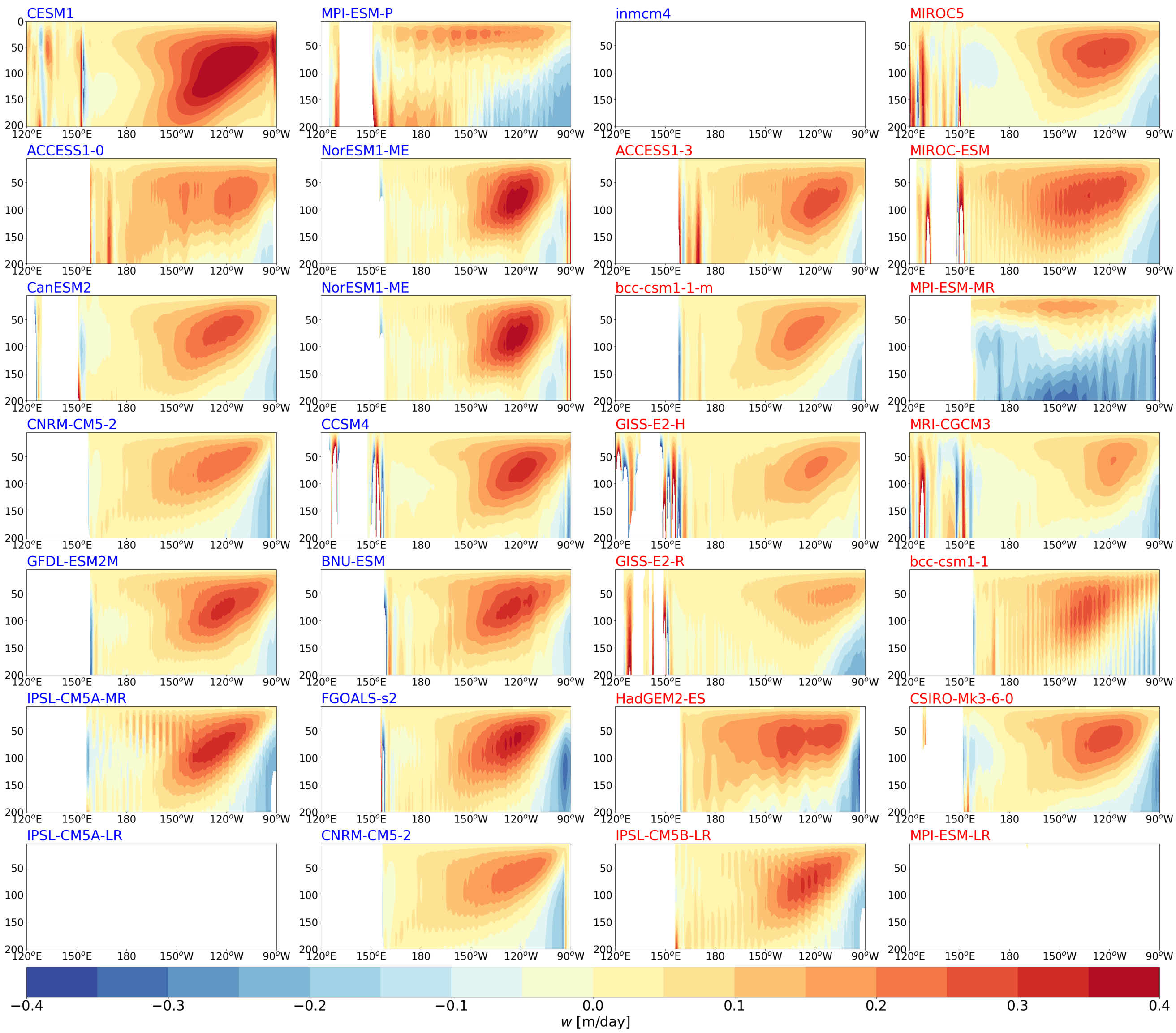

Figure S15. Climatological ocean vertical velocity (m/day) averaged over $5^oS - 5^oN$.

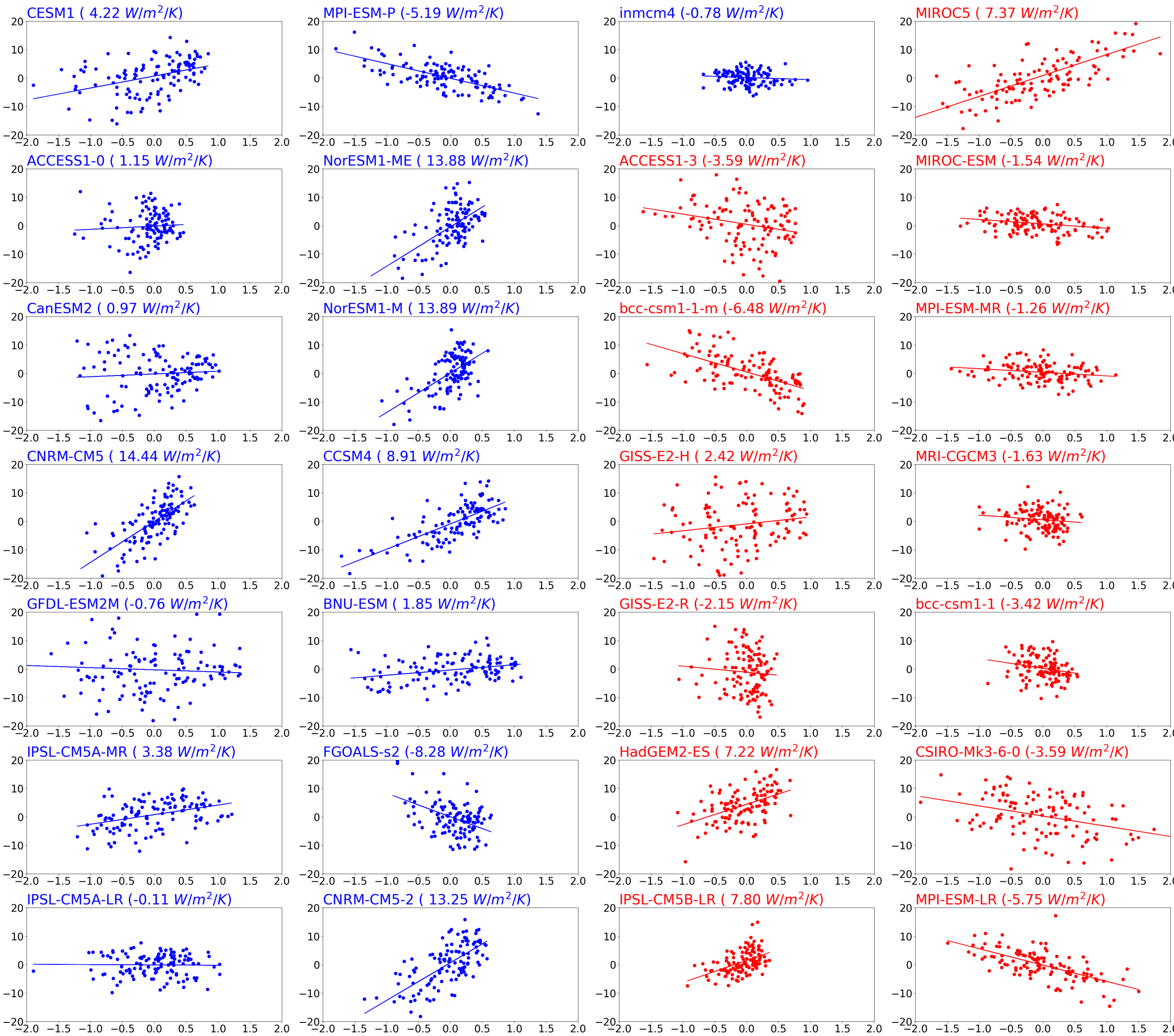

Figure S16. Same as Fig. S12, but for the relationship between SST anomaly and the net downward shortwave radiation anomaly (W/m^2) over $150-270^oE, 5^oS-5^oN$.

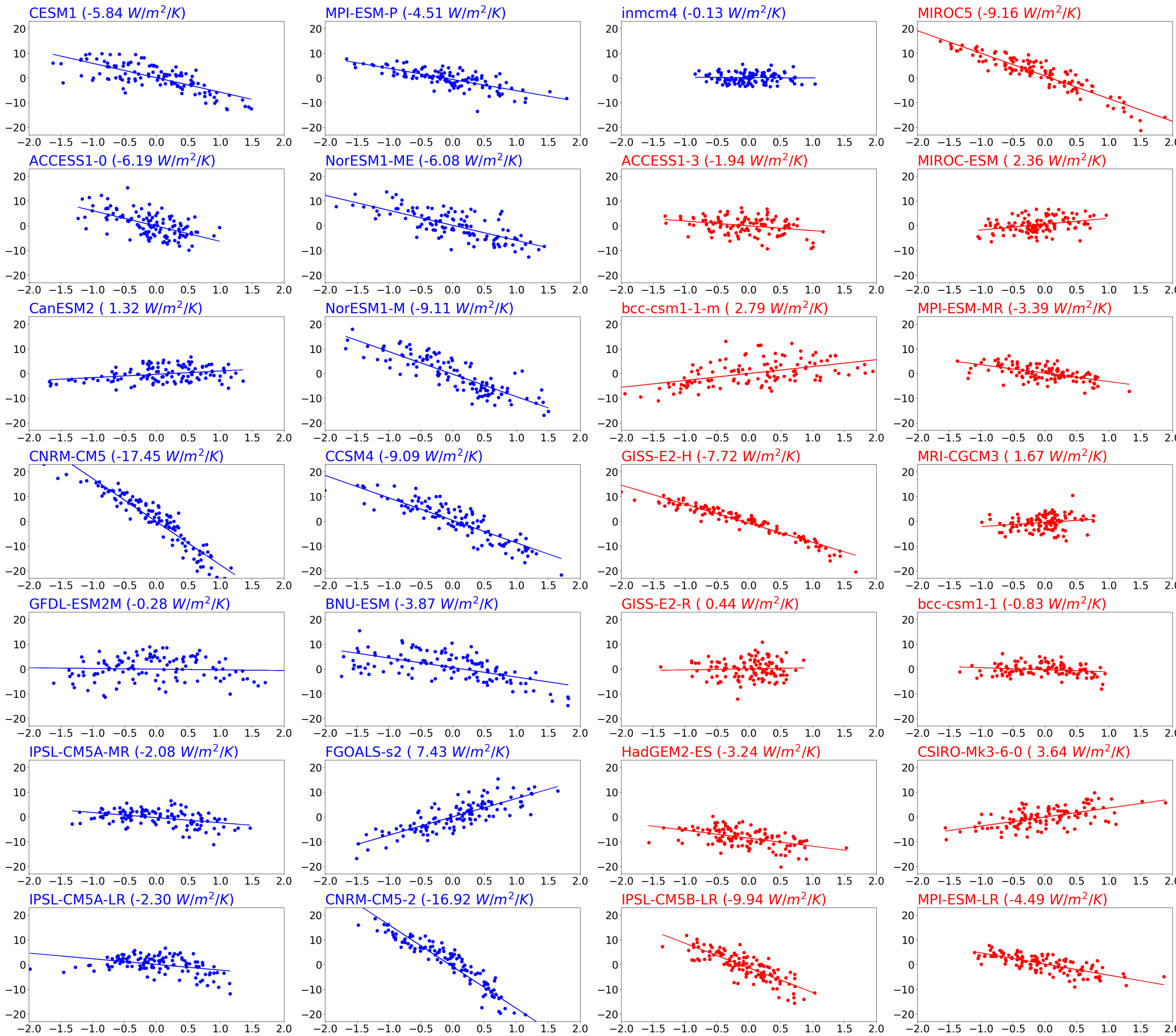

Figure S17. Same as Fig. S12, but for the relationship between SST anomaly and the net downward latent heat flux anomaly (W/m^2) over $150-200^oE, 5^oS-5^oN$.

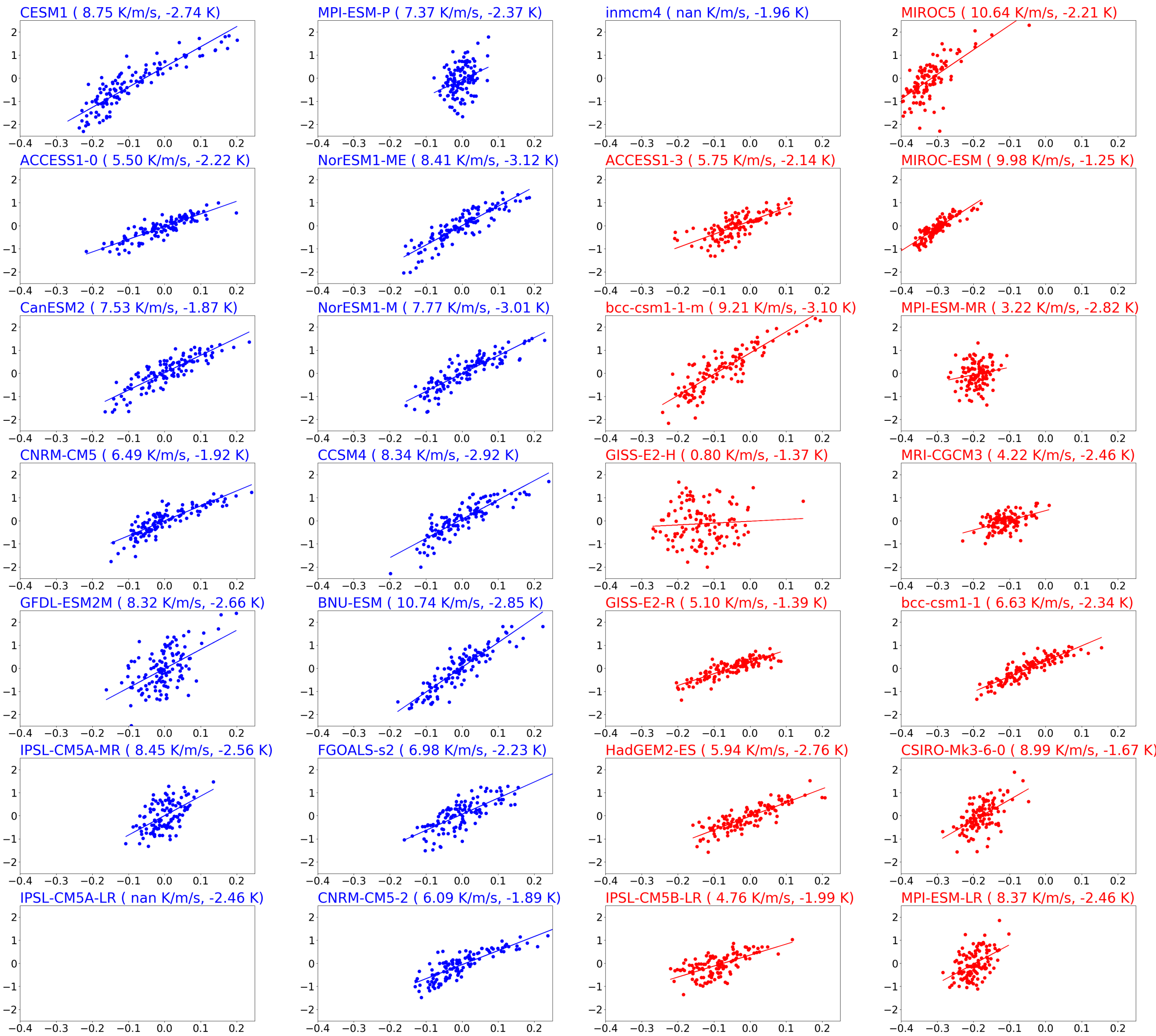

Figure S18. Same as Fig. S12, but for the relationship between column averaged zonal current anomaly (m/s) and SST anomaly over $150 - 270^oE, 5^oS - 5^oN$. The climatological zonal SST gradient is shown as the second number inside of the parentheses.

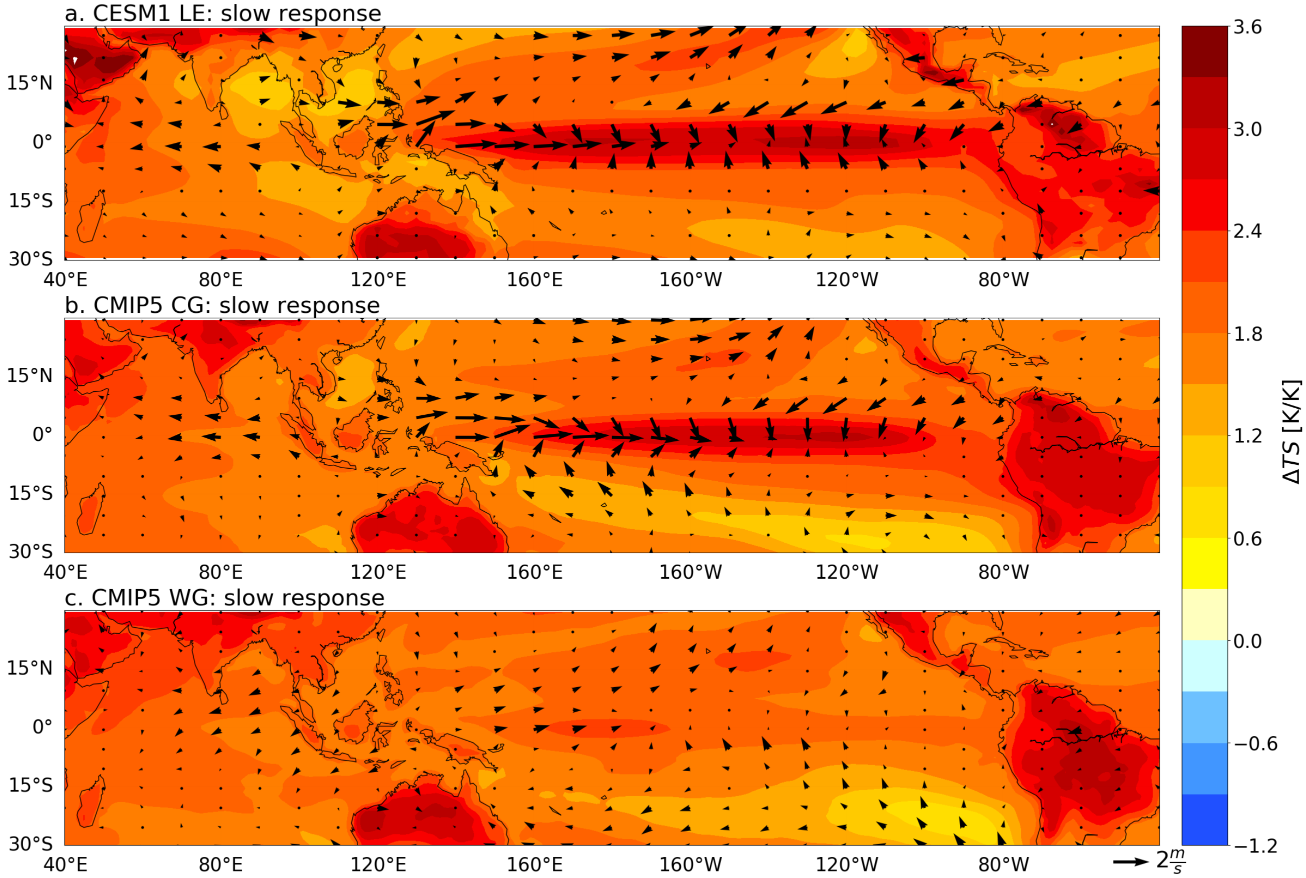

Figure S19. Slow response of TS (shadings) and surface wind (vectors) for CESM1 LE, CMIP5 CG and CMIP5 WG.

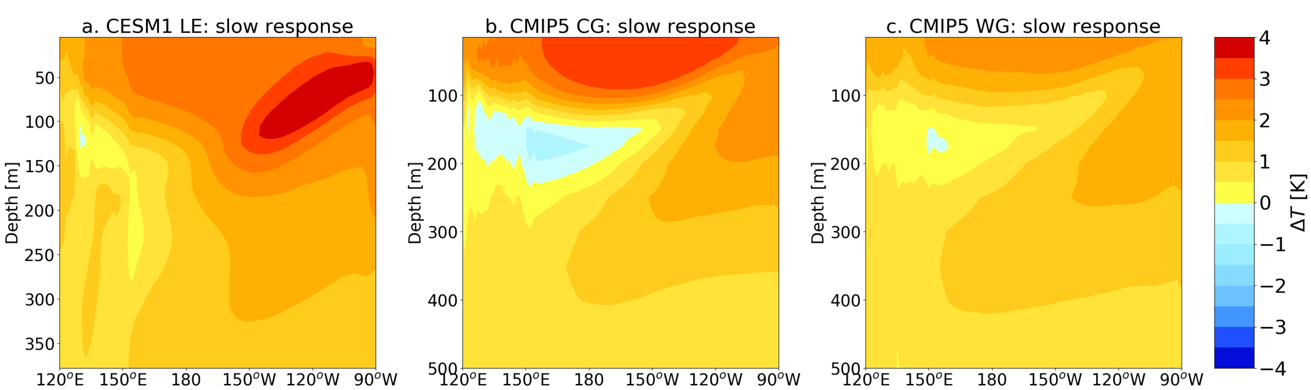

Figure S20. Slow response of equatorial Pacific subsurface ocean temperature (averaged over $5^oS - 5^oN$) for CESM1 LE, CMIP5 CG and CMIP5 WG.

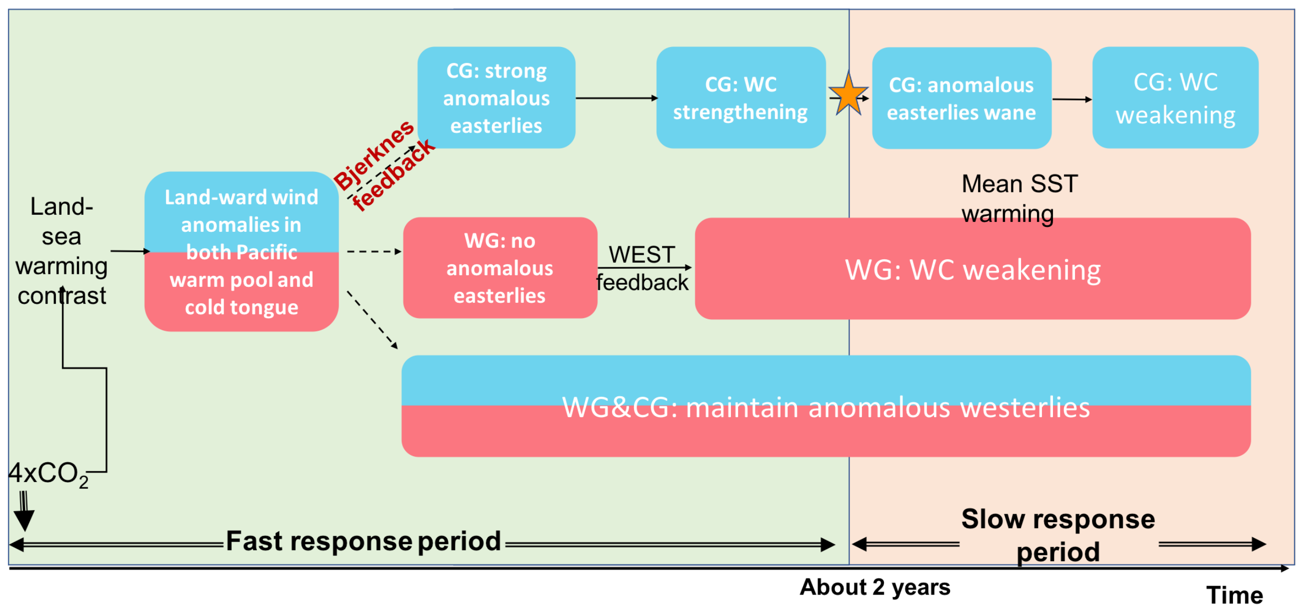

Figure S21. Timeline of the changes in tropical circulation. The single arrow represents "leading to" with the potential mechanisms denoted above; the pink / blue boxes mean the changes in circulation in WG / CG. The box with both colors means this phenomenon exists in both groups. The star sign represents the transition mechanism from fast to slow response period for CG, which is detailed in section 3.2.

Comparison of air-sea coupling strength between CMIP5 models and observations

We calculate the air-sea coupling strength in CMIP5 historical simulations from 1979-2009 and compare it with NCAR/NCEP reanalysis data.

	Bjerknes feedback				Thermal feedback		Zonal advection feedback	
	R(U850, SST) $[\frac{m}{s \cdot K}]$	R(D, U850) [s]	R(Te, D) $[\frac{K}{m}]$	$\overline{w}$ $[m/day]$	R(SW, SST) $[\frac{W}{m^2 \cdot K}]$	R(LH, SST) $[\frac{W}{m^2 \cdot K}]$	R(Uo, SST) $[\frac{K \cdot s}{m}]$	$\delta\overline{SST}$ [K]
Obs	1.65	3.63	0.09	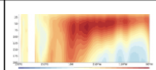	−7.72	3.08	1.45	−2.45
CG	2.25 Err=0.36	2.34 Err=0.36	0.11 Err=0.22	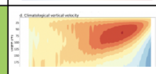	−5.55 Err=0.28	1.09 Err=0.65	10.05 Err=5.93	−2.3 Err=0.06
WG	1.19 Err=0.28	3.14 Err=0.13	0.07 Err=0.22	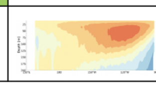	−2.28 Err=0.70	−2.93 Err=1.95	5.18 Err=2.57	−2.06 Err=0.16

$error = |\frac{model - obs}{obs}|$ >0.5 is marked as red

Values closer to observations with error less than 0.5 are shaded with green

Figure S22. Air-sea coupling strength in CMIP5 historical runs for both CG and WG models and observations. The errors between observational and model results are displayed in the second row. Results that are closer to the observations are highlighted in green.